The Impact of Increasing Stratospheric Radiative Damping on the QBO Period

Tiehan Zhou[1,2], Kevin DallaSanta[1,3], Larissa Nazarenko[1,2], Gavin A. Schmidt[1]

[1]NASA Goddard Institute for Space Studies, New York, NY
[2]Center for Climate Systems Research, Columbia University, New York, NY
[3]Universities Space Research Association, Columbia, MD

Correspondence to: Tiehan Zhou (tz2131@columbia.edu)

Abstract. Stratospheric radiative damping increases as atmospheric carbon dioxide concentration rises. We use the one-dimensional mechanistic models of the QBO to conduct sensitivity experiments and find that when atmospheric carbon dioxide concentration increases, the simulated QBO period shortens due to the enhancing of radiative damping in the stratosphere. This result suggests that increasing stratospheric radiative damping due to rising CO_2 may play a role in determining the QBO period in a warming climate along with wave momentum flux entering the stratosphere and tropical vertical residual velocity, both of which also respond to increasing CO_2.

1. Introduction

The quasi-biennial oscillation (QBO) dominates the variability of the equatorial middle and lower stratosphere and is characterized by a downward propagating zonal wind regime that regularly changes from westerlies to easterlies. The QBO period ranges from 22 to 34 months with its average being slightly longer than 28 months. The QBO not only manifests itself in the equatorial zonal winds, but also leaves an imprint on the temperature in both the tropics and extratropics (Baldwin et al., 2001 and references therein).

The QBO has far-reaching implications for global weather and climate systems. First of all, the QBO exerts a marked influence on the distribution and transport of various chemical constituents such as

ozone (O_3) (e.g., Hasebe, 1994), water vapor (H_2O) (e.g., Kawatani et al., 2014), methane (CH_4), nitrous oxide (N_2O), hydrogen fluoride (HF), hydrochloric acid (HC1), odd nitrogen species (NO_y) (e.g., Zawodny and McCormick, 1991), and volcanic aerosol (Trepte and Hitchman, 1992). Secondly, it is well appreciated that the QBO influences the extratropical circulation in the winter stratosphere, which is commonly known as the Holton–Tan effect (Holton and Tan, 1980; Labitzke, 1982). It has been noted that the effect of the QBO on the extratropical winter stratosphere impacts the severity of stratospheric ozone depletion (e.g., Lait et al., 1989). Furthermore, taking account of the QBO improves the simulation and predictability of the extratropical troposphere (e.g., Marshall and Scaife, 2009). Finally, through its modulation of temperature and vertical wind shear in the vicinity of the tropical tropopause, the QBO influences tropical moist convection (Collimore et al., 2003; Liess and Geller, 2012), the El Niño-Southern Oscillation (ENSO) (Gray et al., 1992; Huang et al., 2012; Hansen et al. 2016), the Hadley circulation (Hitchman and Huesmann, 2009), the tropospheric subtropical jet (Garfinkel and Hartmann, 2011a, 2011b), the boreal summer monsoon (Giorgetta et al., 1999), and the Madden-Julian Oscillation (Yoo and Son, 2016**)**. Intriguingly, the QBO is also reported to influence the activities of tropical cyclones (Gray et al., 1984; Ho et al., 2009), albeit this issue is still unsettled (Camargo and Sobel, 2010) and needs further study.

Efforts to understand and simulate the QBO have been ongoing ever since its discovery by Ebdon (1960) and Reed et al. (1961). Lindzen and Holton (1968) and Holton and Lindzen (1972) developed the classical theory of the QBO. Namely, as waves propagate upward, they are attenuated by thermal damping, encounter critical levels, and accelerate and decelerate the mean flow, providing momentum sources for both the westerly and easterly phases of the QBO.

Holton and Lindzen's (1972) model (hereafter referred to as HL model) was further simplified by Plumb (1977), the elegance of which made it a standard paradigm for the QBO. In Plumb's (1977)

Boussinesq formulation, the QBO period is inversely dependent upon both the momentum flux and thermal dissipation rate. Hamilton (1981) further highlighted the role of the radiative damping rate on both the realistic vertical structure and the realistic period of the QBO.

By adopting higher vertical resolutions and incorporating various gravity wave parameterization schemes, many state-of-the-art climate models have shown the capability to self-consistently simulate the QBO (Scaife et al., 2000; Giorgetta et al., 2002, 2006; Rind et al., 2014, 2020; Geller et al., 2016a; Richter et al., 2020a, 2020b). Given the important implications of the QBO for the global climate system, it is natural to ask how the QBO will change in a warming climate.

Giorgetta and Doege (2005) showed a shortening of the QBO period in their doubled CO_2 experiments. They reasoned that both the weakening of the tropical upwelling and the prescribed increase of gravity wave sources lead to the reduction of the QBO period in a warming climate. However, most climate models project a strengthening rather than weakening of tropical upwelling in a warmer climate (Butchart et al., 2006; Butchart 2014; Li et al., 2008). Employing a model without any parametrized non-orographic gravity waves, Kawatani et al. (2011) demonstrated that the intensifying tropical upwelling in a warming climate dominates the counteracting effect of enhanced wave fluxes and consequently projected a lengthening of the QBO period. Using fixed sources of parametrized gravity waves, Watanabe and Kawatani (2012) also projected an elongation of the QBO period in a warming climate and ascribed it to the stronger tropical upwelling. Analyzing four Coupled Model Intercomparison Project phase 5 (CMIP5) models that could simulate a reasonable QBO, Kawatani and Hamilton (2013) found that the projected trends of the QBO period were inconsistent in sign. They further investigated the 60-year operational balloon-borne radiosonde observations provided by the Free Berlin University and detected no significant trend in the QBO period. Richter et al. (2020b) investigated the response of the QBO to doubled and quadrupled CO2 climates among eleven models that participated

112 in Phase 1 of the Stratospheric-tropospheric Processes And their Role in Climate QBO-initiative (QBOi;
113 Butchart et al., 2018), and found no consensus on how the QBO period would respond to a changing
114 climate. Recently, Butchart et al. (2020) evaluated ten Coupled Model Intercomparison Project phase 6
115 (CMIP6) models with realistic QBO in two Shared Socioeconomic Pathways (SSPs, Gidden et al., 2019)
116 scenario simulations and surprisingly found that the QBO period shortens in seven of those ten models
117 in both in both SSP3-7.0 and SSP5-8.5 scenarios although only two and three models show a significant
118 shortening trend in the respective scenarios.

119 It is challenging to ascertain the trend of the QBO period in a warming climate. On one hand, a
120 speeding-up of the Brewer-Dobson circulation in a warming climate leads to a lengthening of the QBO
121 period in most climate models. On the other hand, there is a robust increase in the vertical component of
122 the EP flux for both eastward and westward propagating waves (Richter et al., 2020b; Butchart et al.,
123 2020), indicating that the QBO period shortens due to the enhanced wave driving in a warming climate.
124 The competing effects between enhanced wave driving and a faster Brewer-Dobson circulation suggests
125 that trends in the QBO period are likely to be small and difficult to detect due to the large cycle-to-cycle
126 variability that is reproduced by climate models (Butchart et al., 2020). In addition, uncertainty in the
127 representation of the parameterized gravity waves make it more elusive to detect the trend of the QBO
128 period in a warming climate (Schirber et al., 2015; Richter et al., 2020b).

129 Given the fact that the QBO period is influenced by the radiative damping (Plumb 1977; Hamilton
130 1981), a natural question to ask is whether it could play a role on the trend of the QBO in a warming
131 climate. Plass (1956) showed that when the CO_2 concentration is increased from 330 ppmv to 660 ppmv,
132 the cooling rate increases significantly in the middle and upper stratosphere while it is not changed below
133 the 24 km height level. The cooling rate is increased by more than 50% around the 40 km height level
134 (see his Figure 8).

135 It is well-known that enhanced wave fluxes entering the stratosphere and stronger tropical upwelling
136 individually play a dominant role in determining the trends in the QBO period in a warming climate.
137 Does the competing effect between them leave some room for increasing stratospheric radiative damping
138 to exert an influence on the QBO period? In this paper, we use the HL model to isolate the effect of
139 radiative damping on the QBO period by assuming that the momentum flux entering the stratosphere
140 doesn't change in our experiments. Observational and modeling studies (Andrews et al., 1987; Kawatani
141 et al., 2009, 2010, 2011; Richter et al., 2020b; Holt et al., 2020) showed that the wave forcing spectrum
142 is similar to a discrete two-wave spectrum rather than red-noise or white-noise, all of which are
143 illustrated in Saravanan (1990). Accordingly, the QBO is indeed sensitive to stratospheric radiative
144 damping, and the HL model is suitable for us to conduct the sensitivity analysis.
145 The remainder of this paper is organized as follows. Section 2 investigates the sensitivity of the QBO
146 period to the radiative damping using HL's original model. Section 3 explores the sensitivity of the QBO
147 period to the radiative damping using a modified HL model where the semiannual forcing is removed.
148 Discussion and conclusions are presented in Sections 4 and 5 respectively.
149

150 **2. Sensitivity of the QBO period to enhanced stratospheric radiative damping in the original HL**
151 **model**

152 In the HL model the governing equation of mean flow emerges after the primitive momentum
153 equation is meridionally averaged over some suitable latitudinal belt over the equator.

154 $$\frac{\partial \overline{u}}{\partial t} = -\frac{1}{\rho_0}\frac{\partial}{\partial z}\left[\sum_{i=0}^{1}\overline{F_i}\right] + K_z\frac{\partial^2 \overline{u}}{\partial z^2} + G \qquad (1)$$

where $\overline{u}$ is mean zonal wind, ρ_0 is mean density, $\overline{F_i}$ is the meridionally averaged vertical Eliassen-Palm flux associated with wave i, the index i refers to the individual waves, K_z is a vertical eddy diffusion coefficient, t is time, z is altitude, and G is semiannual forcing identical to that specified by HL.

The $\overline{F_i}$ is are evaluated with Lindzen's (1971) WKB formalism for equatorial waves in shear. When only infrared cooling acts to damp the waves the formulae for $\overline{F_i}$ are

$$\overline{F_0}(z) = A_0\, exp\left(- \int_{17km}^{z} \frac{\alpha N}{k(c-\overline{u})^2}\, dz \right) \tag{2}$$

for the Kelvin wave, and

$$\overline{F_1}(z) = A_1\, exp\left[- \int_{17km}^{z} \frac{\alpha\beta N}{k^3(c-\overline{u})^3}\left(1 - \frac{k^2(\overline{u}-c)}{\beta}\right) dz \right] \tag{3}$$

for the mixed Rossby-gravity wave. As in HL, the wavenumber k, the phase speed c, and A_0 are chosen to be $2\pi/(40{,}000\text{ km})$, 30 m s^{-1}, and 0.04 m^2 s$^{-2}\rho_0$(17 km), respectively for the Kelvin wave while they are equal to $-2\pi/(10{,}000\text{ km})$, -30 m s^{-1}, and -0.04 m^2 s$^{-2}\rho_0$(17 km), respectively for the mixed Rossby-gravity wave. In Eq. (1), $K_z = 0.3$ m^2 s^{-1}, which is also the same as in HL. In addition, $\beta = 2\Omega/a$, where Ω is earth's rotation rate, and a is earth's radius. HL's boundary conditions stipulated that $\overline{u} = 0$ at the lowest model level (17 km) and constrained $\overline{u}$ to vary semiannually at the top level (35 km).

In our control run that is used to depict the present-day QBO all the model parameters are identical to those used by HL in their original simulation. The Brunt-Väisälä frequency

$$N = \sqrt{\frac{g}{T_0}\left(\frac{dT_0}{dz} + \frac{g}{c_p}\right)} \tag{4}$$

In Eq. (4), g is gravity, T_0 is mean temperature, and c_p is specific heat of dry air at constant pressure. HL set N in Eq. (4) to $2.16 \times 10^{-2}\text{s}^{-1}$ with a scale height $H = 6$ km. In addition, the Newtonian

cooling profile in our control run, i.e., $\alpha(z)$ in Eqs. (2) and (3), is also identical to that in the original HL model and depicted in FIG. 1 as the black line. Namely, $\alpha(z)$ in the control run increases from $(21\ \text{day})^{-1}$ at 17 km to $(7\ \text{day})^{-1}$ at 30 km and is kept at $(7\ \text{day})^{-1}$ between 30 km and 35 km. Fels (1985) explicated why this cooling rate is suitable for simulating the QBO on the basis of the scale-dependent effect of radiative damping (Fels 1982). Hamilton (1981) demonstrated that the proper choice of $\alpha(z)$ is crucial in simulating a realistic vertical structure of the QBO.

Eq. (1) was integrated for 100 years using the forward-backward scheme (Matsuno, 1966). The vertical resolution was 250 m and identical to that in HL. The time step was 12 hr, i.e., one half of used in HL, because the 24-hr time step resulted in numerical instability in our integration.

FIG. 2a shows the time–height section of the monthly averaged mean zonal wind simulated over the first 20 years using the HL model. Both the QBO and the semiannual oscillation (SAO) are conspicuous. The fast Fourier transform (FFT) method is used to calculate the frequency power spectra. In order to more accurately derive the QBO period, the model was run for 100 years to increase the spectral resolution. Frequency–height sections of the power spectral densities (PSD) over zero to the Nyquist frequency, i.e., 0.5 cycle/month, depict two sharp lines (peaks) at $\frac{1}{30}$ and $\frac{1}{6}$ cycle/month, respectively (not shown). In order to better visualize the magnitudes of the PSD, we show two truncated frequency–height sections with FIG. 2b and FIG. 2c highlighting the QBO and the SAO respectively. FIG. 2b shows that the QBO dominates over the model domain. The peak frequency corresponds to the period of 30 months. FIG. 2c shows the SAO dominates near the model top due to the fact a semiannual forcing was imposed in the altitudes from 28 to 35 km.

It is worth mentioning that the QBO period shown here is longer than 26.5 months reported in the HL paper (see their FIG. 1). Using the HL model parameters, the QBO period simulated by Plumb (1977) was close to three years (refer to his FIG. 8a), which is longer than our simulated QBO period, i.e., 30.0

months. Although we could not explain why our simulated QBO period is longer than that simulated by HL, we found that when the upper boundary condition is changed from $\overline{u} = 14 \sin(\omega_a t)$ and $\omega_a = \frac{2\pi}{180}$ day^{-1} used in the HL's original model (refer to their Eqs. (2)) to $\frac{\partial \overline{u}}{\partial z} = 0$ used in Plumb (1977), the simulated QBO period becomes 34.3 month (figure not shown). In other words, when we adopted the stress-free upper boundary condition as in Plumb (1977), our simulated QBO period is comparable to that simulated by him, which lends credence to our reconstruction of the HL model.

As mentioned in Section 1, when the atmospheric carbon dioxide concentration is doubled the cooling rate increases significantly in the middle and upper stratosphere while it does not change below the 24 km height level. The cooling rate is increased by more than 50% around the 40 km height level (Plass, 1956). As implied in Dickinson (1973), the estimated cooling coefficient below the 0.2 hPa level is approximately proportional to the estimated cooling rate and is not sensitive to the chosen temperature profile. In other words, the relative increase in the cooling coefficient is roughly equal to the relative increase in the cooling rate as the CO_2 concentration is doubled. Accordingly, the Newtonian cooling profile in our experimental run, i.e., $\alpha(z)$ in Eqs. (2) and (3), is specified in FIG. 1 as the red line. Namely, $\alpha(z)$ in the experimental run increases from $(21 \text{ day})^{-1}$ at 17 km to $\frac{9}{91}$day^{-1} at 24 km, which is identical to that in the control run from 17 km to 24 km. We increased $\alpha(z)$ in the experimental run between 30 km and 35 km by 30% relative to that in the control run. In other words, $\alpha(z)$ is kept at $\frac{1.3}{7}$day^{-1} between 30 km and 35 km in the experimental run. This percentage increase of 30% in $\alpha(z)$ for the doubled CO_2 above 30 km shown in FIG. 1 is somewhat less than that implied in the Figure 8 of Plass (1956), because we would like our estimated relative increase in $\alpha(z)$ to err on the conservative side given the inherent uncertainties mentioned by him. Between 24 km and 30 km, $\alpha(z)$ in the experimental run is formulated linearly with height from $\frac{9}{91}$day^{-1} at 24 km to at $\frac{1.3}{7}$day^{-1} at 30 km.

FIG. 3a shows the time–height section of the monthly averaged mean zonal wind simulated over the first 20 years for the doubled CO_2 run, where the increased $\alpha(z)$ depicted as the red line in FIG. 1 was employed while all other parameters are identical to those in the control run. Obviously, the QBO dominates below 28 km while the semiannual oscillation (SAO) dominates above 31 km. Like FIG. 2b and FIG. 2c, we only show two truncated frequency–height sections with FIG. 3b highlighting the QBO and FIG. 3c highlighting the SAO. FIG. 3b also shows that the QBO prevails over the model domain. The peak frequency corresponds to the period of 27.9 months. FIG. 3c shows the SAO dominates near the model top due to the same imposed semiannual forcing as that in the control run.

In summary, using the original HL model we found that the increased radiative damping due to the doubling of CO2 shortens the QBO period by 7% (i.e., decreases from 30 months to 27.9 months).

3. Sensitivity of the QBO period to enhanced stratospheric radiative damping in the HL model without the semiannual forcing

HL pointed out that the imposed semiannual oscillation was not essential for their QBO theory. Applying $\frac{\partial \overline{u}}{\partial z} = 0$ as the upper boundary condition, Plumb (1977) showed a simulated QBO without resorting to the semiannual momentum source (refer to his FIG. 8b). In the following control run, all parameters are identical to those used in the previous control run in Section 2 except that G in Eq. (1) is set to zero with $\frac{\partial \overline{u}}{\partial z}$ also being set to zero at $z = 35$ km. Hereafter we refer to it as the Plumb model[1]. FIG. 4a shows the time–height section of the monthly averaged mean zonal wind simulated over the first 20 years using the Plumb model. As expected, the QBO emerges without any trace of SAO since $G = 0$ in Eq. (1). FIG. 4b shows that the QBO dominates over the whole model domain. The peak frequency

[1] Strictly speaking, it is the HL model modified by Plumb (1977). In this paper, we don't use his eponymous model, i.e., the simplest possible model of the QBO, where Boussinesq fluids with uniform mean density were employed, because the HL model and its variant are considerably more realistic.

corresponds to the period of 37.5 months, which is comparable to that simulated by Plumb (1977) shown in his FIG. 8b. Apparently, the QBO period from the Plumb model, i.e., 37.5 months shown in FIG. 4b, is longer than that from the HL model, i.e., 30.0 months shown in FIG. 2b. This is partly because the additional forcing G in Eq. (1) was removed in the Plumb model.

In the following experimental run, all parameters are identical to those used in the previous experimental run in Section 2 except that G in Eq. (1) is set to zero with $\frac{\partial \overline{u}}{\partial z}$ also being set to zero at $z = 35\ \mathrm{km}$. In other words, the following experimental run using the Plumb model employed the same parameters as the afore-mentioned control run using the Plumb model except that the increased $\alpha(z)$ shown as the red line in FIG. 1 was used in the following experimental run while $\alpha(z)$ shown as the black line in FIG. 1 was used in the above control run. FIG. 5a shows the time–height section of the monthly averaged mean zonal wind simulated over the first 20 years for the doubled CO_2 run. It is natural that only the QBO emerges. A comparison of FIG. 4a and FIG. 5a shows that the QBO period shortens when the infrared damping increases in response to the doubled CO2. FIG. 5b shows that the QBO dominates over the whole model domain. The peak frequency corresponds to the period of 31.6 months.

Using the Plumb model, we found that the increased radiative damping due to the doubling of CO_2 shortens the QBO period by 15.7% (i.e., decreases from 37.5 months to 31.6 months).

4. Discussion

The semiannual forcing, G in Eq. (1), in the HL model is imposed rather than results from the wave-flow interaction. In other words, G in Eq. (1) is independent of mean flow, and is specified as $G = 0$ for $z \leq 28\ \mathrm{km}$, and $G = \omega_{sa}\overline{u}_{sa}$ for $z > 28\ \mathrm{km}$

where $\overline{u}_{sa} = 2(z - 28\text{km})\ \text{m s}^{-1}\ \text{km}^{-1}\sin(\omega_{sa}t)$ and $\omega_{sa} = \frac{2\pi}{180}\ \text{day}^{-1} \approx 4 \times 10^{-7}\ \text{s}^{-1}$ (refer to Eqs. (2) in HL). Therefore, we have $\frac{\partial^2 \overline{u}_{sa}}{\partial z^2} = 0$ in the HL original model. We furthermore decompose $\overline{u}$ into two components: $\overline{u}_{QBO}\ and\ \overline{u}_{sa}$. Combining Eq. (1), the decomposition of $\overline{u}\ as\ \overline{u} = \overline{u}_{QBO} + \overline{u}_{sa}$, the above-mentioned $\frac{\partial^2 \overline{u}_{sa}}{\partial z^2} = 0$, and $G = \omega_{sa}\overline{u}_{sa} = \frac{\partial \overline{u}_{sa}}{\partial t}$ for $z > 28$ km, yields

$$\frac{\partial \overline{u}_{QBO}}{\partial t} = -\frac{1}{\rho_0}\frac{\partial}{\partial z}\left[\sum_{i=0}^{1}\overline{F_i}\right] + K_z\frac{\partial^2 \overline{u}_{QBO}}{\partial z^2} \tag{5}$$

for $z > 28$ km.

Dunkerton (1997) showed that in the presence of tropical upwelling it was gravity waves rather than large-scale Kelvin and mixed Rossby-gravity waves that contributed the bulk of QBO forcing. Consequently, Geller et al. (2016a, 2016b) pointed out that enough gravity wave momentum flux is required to model the QBO in a self-consistent manner in climate models and that the magnitude of the subgrid-scale gravity wave momentum flux plays a crucial role in determining the QBO period. Since there is no tropical upwelling in either the HL model or the Plumb model, and the semiannual forcing, G, is dependent on neither $\overline{u}$ in Eq. (1) nor $\overline{u}_{QBO}$ in Eq. (5), it is natural that planetary-scale Kelvin and mixed Rossby-gravity waves largely determine the QBO periods shown in Sections 2 and 3 due to the fact that G only exerts a weak influence on the planetary wave forcing, i.e., $-\frac{1}{\rho_0}\frac{\partial}{\partial z}\left[\sum_{i=0}^{1}\overline{F_i}\right]$ in Eqs. (1) and (5). We conducted another sensitivity test where all parameters are identical to those in the HL model except that G in both the control and experimental runs is twice as large as that used by HL. As the radiative damping profile changes from the black line to the red line above 24 km shown in FIG. 1, our simulated QBO period decreases from 28.6 months to 27.3 months (figures not shown). This smaller percentage decrease of 4.5% is not unexpected because the unrealistically larger G that is independent of $\overline{u}$ makes the model atmosphere less sensitive to the changes in the radiative damping.

283 We further conducted two sensitivity tests where all parameters are identical to those in the HL model
284 except that G in the first test is half as large as that used by HL and is equal to zero in the second test.
285 Surprisingly, as the radiative damping profile changes from the black line to the red line above 24 km
286 shown in FIG. 1, our simulated QBO periods decreases from 30.0 months to 28.6 months both for G
287 being decreased by 50% and for $G = 0$ (figures not shown). This 4.7% decrease in the QBO period is
288 somewhat smaller than the 7% reduction obtained from the sensitivity test presented in Section 2 when
289 G is the same as that used by HL. It is surprising because the model atmosphere is expected to be more
290 sensitive to the changes in the radiative damping as G, which is independent of $\overline{u}$, becomes smaller and
291 smaller. Note that when our control runs adopt the black radiative damping profile shown in FIG. 1 the
292 simulated QBO periods are not sensitive to the imposed semiannual forcing provided that G does not
293 exceed the values employed by HL. Similarly, when our experimental runs adopt the red radiative
294 damping profile above 24 km shown in FIG. 1 the simulated QBO periods are also not sensitive to the
295 imposed semiannual forcing provided that G does not exceed 50% of the values adopted in HL. The
296 question naturally arises: what is responsible for this unphysical behavior?
297 In Section 2, the simulated QBO periods are equal to 30 and 34.3 months when we adopted the no-
298 slip and stress-free upper boundary condition respectively with all other parameters being identical to
299 those used by HL. The results implicate the upper boundary conditions in the inconsistency. Plumb (1977)
300 pointed out that the upper boundary in HL was undesirably low and implied that raising the lid to an
301 additional 50% would be adequate for the robustness in his model. Here, we carry out a series of
302 sensitivity tests by raising the model lid gradually from 35 km to 55 km with the one-kilometer increment.
303 we will demonstrate how the behavior of the HL model with $G = 0$ converges with that of the Plumb
304 model. The modified HL model, i.e., the HL model with $G = 0$ is identical to the Plumb model except
305 that the former has the no-slip upper boundary condition while the latter has the stress-free upper

boundary condition. Both models share the same governing equation (5). Note that we set the radiative damping rate above the 35 km level to its value at the 35 km level shown in FIG. 1.

For the radiative damping profile corresponding to the reference CO_2, FIG. 6 shows that when the model lid is placed at the 35 km level the simulated QBO period of 30.0 months with the no-slip upper boundary condition (solid black line) is apparently shorter than that of 37.5 months with the stress-free upper boundary condition (dashed black line). FIG. 6 also shows that as the model lid is raised incrementally from the 35 km level to the 46 km level, the discrepancies between the simulated QBO periods due to the different upper boundary conditions decrease monotonically. No matter whether we adopt the no-slip or stress-free upper boundary condition, the simulated QBO period is 32.4 months for the reference radiative damping profile provided that the model top is at or above the 46 km level.

Similarly, for the radiative damping profile corresponding to the doubled CO_2, FIG. 6 demonstrates that when the model lid is placed at the 35 km level the simulated QBO period of 28.6 months with the no-slip upper boundary condition (solid red line) is obviously shorter than that of 31.6 months with the stress-free upper boundary condition (dashed red line). FIG. 6 also exhibits that as the model lid is raised gradually from the 35 km level to the 40 km level, the discrepancies between the simulated QBO periods due to the different upper boundary conditions decrease monotonically. No matter whether we adopt the no-slip or stress-free upper boundary condition, the simulated QBO period for the enhanced infrared cooling due to the doubled CO_2 is 30.0 months provided that the model top is at or above the 40 km level. It is apparent that the required model top is lower when the radiative damping is augmented due to the doubling of CO_2 because the planetary waves dissipate more steeply with height in presence of the enhanced infrared cooling rates.

FIG. 6 suggests that when the model lid is sufficiently high the QBO period in response to the enhanced radiative damping due to the increasing CO_2 will decrease from 32.4 to 30.0 months. This

329 7.4% decrease in the QBO period is independent of the upper boundary condition. Plass (1956) indicated
330 that the probable error of the cooling rate was about 10% below 20 km, increasing to 30% at 50 km and
331 that the relative differences between the cooling rates should be considerably more accurate than their
332 magnitude. In other words, the relative differences between the various cooling rates calculated by Plass
333 (1956) should be considerably smaller 30%. Using the HL model with its top at the 48 km level, we
334 further conducted two experiments by adopting $G = 0$ in Eq. (1) and increasing the radiative damping
335 corresponding to the doubled CO_2 between 30 km and 48 km by $30\% - 30\% * 30\% = 21\%$ and
336 $30\% + 30\% * 30\% = 39\%$ respectively relative to that in the control run. The simulated QBO periods
337 are 30.8 and 29.3 months respectively. Therefore, when the model lid is sufficiently high the QBO period
338 in response to the enhanced radiative damping due to the doubled CO_2 will decrease by approximately
339 $7.4\% \pm 2.5\%$.

340 Note that N, the Brunt-Väisälä frequency, in Eqs. (2) and (3) also changes with increasing CO_2.
341 Richter et al. (2020b) showed that N^2 would be decreased by $\sim 5\%$ in the stratosphere when CO_2 is
342 doubled (refer to their Figure 2c). We used the HL model to conduct a sensitivity test by adopting $G = 0$
343 in Eq. (1) with the radiative damping profile corresponding to the doubled CO_2 and the top of the models
344 at the 48 km level. The rest of parameters in this sensitivity test are identical to those in all the previous
345 runs except that the Brunt-Väisälä frequency in this experimental run was 2.5% smaller than that in the
346 control run. The models were run for 1000 years to further increase the spectral resolution. We found
347 that when the Brunt-Väisälä frequency was decreased by 2.5%, the simulated QBO period was slightly
348 lengthened from 30 months to 30.2 months (figure not shown). In other words, the impact of decreasing
349 stratospheric buoyancy frequency on the QBO period is marginal.

350 Analyzing eleven CCMI-1 REF-C2 climate–chemistry simulations, Eichinger and Šácha (2020)
351 showed that the scale height in the stratosphere decreases by 2.3% per century. Accordingly, we used

the HL model to conduct another sensitivity test by adopting $G = 0$ in Eq. (1) with the radiative damping profile corresponding to the doubled CO_2 and the top of the models at the 48 km level. The rest of parameters in this sensitivity test are identical to those in all the previous control runs except that the scale height in this experimental run was 2.3% smaller than that in the control run. The model was also run for 1000 years for the sake of higher spectral resolution. We found that when the scale height was decreased by 2.3%, the simulated QBO period was also shortened by about 2.3%, i.e., from 30 months to 29.3 months (figure not shown). Apparently, the shortening of the QBO period due to the warming climate is ascribed less to the shrinkage of the scale height in the stratosphere than to the enhancing of the stratospheric radiative damping. Together, the shrinking scale height and the increasing radiative damping shorten the QBO period by about 9.6%.

5. Conclusions

Plumb (1977) envisioned that stratospheric climate change would give rise to long-term changes in the QBO period due to changes in radiative damping and the Brunt-Väisälä frequency. Using one-dimensional (1D) models we found that the enhanced radiative damping arising from the doubling of CO2 leads to the shortening of the QBO period by about $7.4\% \pm 2.5\%$ provided that the model top is higher than the 46 km level. Furthermore, when we incorporated both the 2.3% shrinkage of the scale height and the enhanced radiative damping, the QBO period is shortened by about 9.6%. In addition, the impact of decreasing stratospheric buoyancy frequency on the QBO period is marginal. Note that those models include neither gravity waves nor tropical upwelling and assume that there are no changes in wave fluxes entering the equatorial stratosphere.

From a comprehensive model perspective, Richter et al. (2020b) showed that the changes in period of the QBO in warming climate simulations varied quite significantly among these models. Some models

projected longer mean periods and some shorter mean periods for the QBO in a future warmer climate. They argue that uncertainty in the representation of the parameterized gravity waves is the most likely cause of the spread among the QBOi models in the QBO's response to climate change.

In addition, CO2 increases in the NASA Goddard Institute for Space Studies Model E2.2-AP (Rind et al. 2020) lead to a decrease of both QBO period and QBO amplitude (DallaSanta et al., in prep.). The period decrease is associated with increases in lower stratospheric momentum fluxes (related to parameterized convection), a finding consistent with Geller et al. (2016a, 2016b) and Richter et al. (2020b). The amplitude decrease is associated with a strengthened residual mean circulation, also consistent with the literature, although the vertical structure of the circulation response is nontrivial. It is worth mentioning that horizontal momentum flux divergences could also play an important role in weakening the QBO (Match and Fueglistaler, 2019, 2020).

Our 1D models only explored how the QBO period responds to the enhancing radiative damping of planetary waves, the shrinking scale height in the stratosphere, and the decreasing stratospheric buoyancy frequency due to the increasing CO_2 concentration. In order to investigate how those factors affect gravity waves which play an even more important role in determining the QBO period than planetary waves, high-resolution models such as those used by Kawatani et al. (2011, 2019) are desirable to further our understanding. Ultimately, how the QBO period changes in response to the increasing CO_2 will be determined by the combined effects of the strengthening of tropical upwelling, the increasing of wave fluxes entering the equatorial stratosphere, the enhancing of radiative damping, and the shrinking of the scale height in the stratosphere, which warrants further research.

Acknowledgements: Climate modeling at GISS is supported by the NASA Modeling, Analysis and Prediction program, and resources supporting this work were provided by the NASA High-End

398 Computing (HEC) Program through the NASA Center for Climate Simulation (NCCS) at Goddard Space
399 Flight Center. KD acknowledges support from the NASA Postdoctoral Program. The authors also
400 acknowledge very useful discussions with Drs. Geller and Clara Orbe.
401

402 **References**

403 Andrews, D. G., Holton, J. R., and Leovy, C. B.: Middle Atmosphere Dynamics, Academic Press, 489
404 pp, 1987.

405 Baldwin, M. P., Gray, L. J., Dunkerton, T. J., Hamilton, K., Haynes, P. H., Randel, W. J., Holton, J. R.,
406 Alexander, M. J., Hirota, I., Horinouchi, T., Jones, D. B. A., Kinnersley, J. S., Marquardt, C., Sato,
407 K., and Takahashi, M.: The Quasi-biennial oscillation, Rev. Geophys., 39, 179–229,
408 https://doi.org/10.1029/1999RG000073, 2001.

409 Butchart, N.: The Brewer-Dobson circulation, Rev. Geophys., 52, 157–
410 184, https://doi.org/10.1002/2013RG000448, 2014.

411 Butchart, N., Scaife, A. A., Bourqui, M., Grandpré, J., Hare, S. H., Kettleborough, J., Langematz, U.,
412 Manzini, E., Sassi, F., Shibata, K., Shindell, D. and Sigmond, M.: Simulations of anthropogenic
413 change in the strength of the Brewer–Dobson circulation, Climate Dynamics, 27, 727–741,
414 https://doi.org/10.1007/s00382-006-0162-4, 2006.

415 Butchart, N., Anstey, J., Hamilton, K., Osprey, S., McLandress, C., Bushell, A. C., Kawatani, Y., Kim,
416 Y.-H., Lott, F., Scinocca, J., Stockdale, T.N., Andrews, M., Bellprat, O., Braesicke, P., Cagnazzo,
417 C., Chen, C.-C., Chun, H.-Y., Dobrynin, M., Garcia, R., Garcia-Serrano, J., Gray, L.J., Holt, L.,
418 Kerzenmacher, T., Naoe, H., Pohlmann, H., Richter, J. H., Scaife, A.A., Schenzinger, V., Serva, F.,
419 Versick, S., Watanabe, S., Yoshida, K. and Yukimoto, S.: Overview of experiment design and
420 comparison of models participating in phase 1 of the SPARC Quasi-Biennial Oscillation initiative

(QBOi), Geoscientific Model Development, 11, 1009–1032. https://doi.org/10.5194/gmd-11-1009-2018, 2018.

Butchart, N., Anstey, J. A., Kawatani, Y., Osprey, S. M., Richter, J. H., Wu, T.: QBO changes in CMIP6 climate projections, *Geophys. Res. Lett.,* 47, 1–10. https://doi.org/10.1029/2019GL086903, 2020.

Camargo, S. J. and Sobel, A. H.: Revisiting the influence of the quasi-biennial oscillation on tropical cyclone activity, J. Climate, 23, 5810–5825, https://doi.org/10.1175%2F2010JCLI3575.1, 2010.

Collimore, C. C., Martin, D. W., Hitchman, M. H., Huesmann, A., and Waliser, D. E.: On the relationship between the QBO and tropical deep convection, J. Climate, 16, 2552–2568, https://doi.org/10.1175/1520-0442(2003)016%3C2552:OTRBTQ%3E2.0.CO;2, 2003.

Dickinson, R. E.: Method of parameterization for infrared cooling between altitudes of 30 and 70 kilometers, J. Geophys. Res., 78, 4451–4457, https://doi.org/10.1029/JC078i021p04451, 1973.

Dunkerton, T. J.: The role of gravity waves in the quasi-biennial oscillation, J. Geophys. Res., 102, 26053–26076, https://doi.org/10.1029/96JD02999, 1997.

Ebdon, R. A.: Notes on the wind flow at 50mb in tropical and subtropical regions in January 1957 and in 1958, Q. J. Roy. Meteor. Soc., 86, 540–542, https://doi.org/10.1002/qj.49708637011, 1960.

Eichinger, R. and Šácha, P.: Overestimated acceleration of the advective Brewer-Dobson circulation due to stratospheric cooling, Q. J. R. Meteorol. Soc., 1-15, https://doi.org/10.1002/qj.3876, 2020.

Fels, S. B.: A parameterization of scale-dependent radiative damping rates in the middle atmosphere, J. Atmos. Sci., 39, 1141–1152, https://doi.org/10.1175/1520-0469(1982)039%3C1141:APOSDR%3E2.0.CO;2, 1982.

Fels, S. B.: Radiative-dynamical interactions in the middle atmosphere, Advances in Geophysics, Vol. 28A, Academic Press, 277–300, https://doi.org/10.1016/S0065-2687(08)60227-7, 1985.

Garfinkel, C. I. and Hartmann, D. L.: The influence of the quasi-biennial oscillation on the troposphere in winter in a hierarchy of models. Part I: Simplified dry GCMs, J. Atmos. Sci., 68, 1273–1289, https://doi.org/10.1175%2F2011JAS3665.1, 2011a.

Garfinkel, C. I. and Hartmann, D. L.: The influence of the quasi-biennial oscillation on the troposphere in winter in a hierarchy of models. Part II: Perpetual winter WACCM runs, J. Atmos. Sci., 68, 2026–2041, https://doi.org/10.1175%2F2011JAS3702.1, 2011b.

Geller, M. A., Zhou, T., Shindell, D., Ruedy, R., Aleinov, I., Nazarenko, L., Tausnev, N. L., Kelley, M., Sun, S., Cheng, Y., Field, R. D., and Faluvegi, G.: Modeling the QBO-improvements resulting from higher-model vertical resolution, J. Adv. Model. Earth Syst., 8, 1092–1105, https://doi.org/10.1002/2016MS000699, 2016a.

Geller, M. A., Zhou, T., and Yuan, W.: The QBO, gravity waves forced by tropical convection, and ENSO, J. Geophys. Res. Atmos., 121, 8886-8895, https://doi.org/10.1002/2015JD024125, 2016b.

Gidden, M. J., Riahi, K., Smith, S. J., Fujimori, S., Luderer, G., Kriegler, E., van Vuuren, D. P., van den Berg, M., Feng, L., Klein, D., Calvin, K., Doelman, J. C., Frank, S., Fricko, O., Harmsen, M., Hasegawa, T., Havlik, P., Hilaire, J., Hoesly, R., Horing, J., Popp, A., Stehfest, E., and Takahashi, K.: Global emissions pathways under different socioeconomic scenarios for use in CMIP6: a dataset of harmonized emissions trajectories through the end of the century, Geosci. Model Dev., 12, 1443–1475, https://doi.org/10.5194/gmd-12-1443-2019, 2019.

Giorgetta, M. A. and Doege, M. C.: Sensitivity of the Quasi-Biennial Oscillation to CO_2 doubling, Geophys. Res. Lett., 32, L08701. https://doi.org/10.1029/2004GL021971, 2005.

Giorgetta, M. A., Bengtson, L., and Arpe, K.: An investigation of QBO signals in the east Asian and Indian monsoon in GCM experiments, Climate Dynamics, 15, 435–450, https://doi.org/10.1007/s003820050292, 1999.

Giorgetta, M. A., Manzini, E., and Roeckner, E.: Forcing of the quasi-biennial oscillation from a broad spectrum of atmospheric waves, *Geophys. Res. Lett.*, 29, https://doi.org/10.1029/2002GL014756, 2002.

Giorgetta, M. A., Manzini, E., and Roeckner, E., Esch, M., and Bengtsson, L.: Climatology and forcing of the quasi-biennial oscillation in the MAECHEM5 model, J. Climate, 19, 3882–3901, https://doi.org/10.1175/JCLI3830.1, 2006.

Gray, W. M.: Atlantic seasonal hurricane frequency. Part I: El Niño and 30-mb quasi-biennial oscillation influences, Mon. Wea. Rev., 112, 1649–1688, https://doi.org/10.1175/1520-0493(1984)112%3C1649:ASHFPI%3E2.0.CO;2, 1984.

Gray, W. M., Sheaffer, J. D., and Knaff, J.: Influence of the stratospheric QBO on ENSO variability, J. Meteor. Soc. Jpn., 70, 975–995, https://doi.org/10.2151/jmsj1965.70.5_975, 1992.

Hamilton, K.: The vertical structure of the quasi-biennial oscillation: Observations and theory, Atmos. Ocean, 19, 236–250, http://dx.doi.org/10.1080/07055900.1981.9649111, 1981.

Hansen, F., Matthes, K., and Wahl, S.: Tropospheric QBO–ENSO interactions and differences between the Atlantic and Pacific, J. Climate, 29, 1353–1368, https://doi.org/10.1175/JCLI-D-15-0164.1, 2016

Hasebe, F.: Quasi-biennial oscillations of ozone and diabatic circulation in the equatorial stratosphere, J. Atmos. Sci., 51, 729–745, https://doi.org/10.1175/1520-0469(1994)051%3c0729:QBOOOA%3e2.0.CO;2, 1994.

Hitchman, M. H., and Huesmann, A. S.: Seasonal influence of the quasi-biennial oscillation on stratospheric jets and Rossby wave breaking, J. Atmos. Sci., 66, 935–946, https://doi.org/10.1175%2F2008JAS2631.1, 2009.

Ho, C.-H., Kim, H.-S., Jeong, J.-H., and Son, S.-W.: Influence of stratospheric quasi-biennial oscillation on tropical cyclone tracks in the western North Pacific, Geophys. Res. Lett., 36, L06702, http://dx.doi.org/10.1029/2009GL037163, 2009.

Holt, L., Lott, F., Garcia, R., Kiladis, G.N., Anstey, J.A., Braesicke, P., Bushell, A.C., Butchart, N., Cagnazzo, C., Chen, C.-C., Chun, H.-Y., Hamilton, K., Kawatani, Y., Kerzenmacher, T., Kim, Y.-H., McLandress, C., Naoe, H., Osprey, S., Richter, J.H., Scinocca, J., Serva, F., Versick, S., Watanabe, S., Yoshida, K., and Yukimoto, S.: An evaluation of tropical waves and wave forcing of the QBO in the QBOi models, Q. J. R. Meteorol. Soc., https://doi.org/10.1002/qj.3827, 2020.

Holton, J. R. and Lindzen, R. S.: An updated theory for the quasi-biennial cycle of the tropical stratosphere, J. Atmos. Sci., 29, 1076–1080, https://doi.org/10.1175/1520-0469(1972)029%3c1076:AUTFTQ%3e2.0.CO;2, 1972.

Holton, J. R. and Tan, H.: The Influence of the equatorial quasi-biennial oscillation on the global circulation at 50 mb, J. Atmos. Sci., 37, 2200–2208, https://doi.org/10.1175/1520-0469(1980)037%3c2200:TIOTEQ%3e2.0.CO;2, 1980.

Huang, B. H., Hu, Z. Z., Kinter, J. L., Wu, Z. H., and Kumar, A.: Connection of stratospheric QBO with global atmospheric general circulation and tropical SST. Part I: Methodology and composite life cycle, Climate Dynamics, 38, 1–23, https://doi.org/10.1007%2Fs00382-011-1250-7, 2012.

Kawatani, Y. and Hamilton, K.: Weakened stratospheric Quasi-Biennial Oscillation driven by increased tropical mean upwelling, Nature, 497, 478–481, https://doi.org/10.1038/nature12140, 2013.

Kawatani, Y., Takahashi, M., Sato, K., Alexander, S. P., and Tsuda, T.: Global distribution of atmospheric waves in the equatorial upper troposphere and lower stratosphere: AGCM simulation of sources and propagation, J. Geophys. Res., 114, D01102, https://doi.org/10.1029/2008JD010374, 2009.

Kawatani, Y., Watanabe, S., Sato, K., Dunkerton, T. J., Miyahara, S., and Takahashi, M.: The roles of equatorial trapped waves and internal inertia-gravity waves in driving the Quasi-Biennial oscillation. Part I: Zonal mean wave forcing, J. Atmos. Sci., 67, 963–980, https://doi.org/10.1175/2009JAS3222.1, 2010.

Kawatani, Y., Hamilton, K., and Watanabe, S.: The quasi-biennial oscillation in a double CO2 climate, J. Atmos. Sci., 68, 265–283, https://doi.org/10.1175/2010JAS3623.1, 2011.

Kawatani, Y, Lee, J. N., and Hamilton, K.: Interannual variations of stratospheric water vapor in MLS observations and climate model simulations, J. Atmos. Sci., 71, 4072–4085, https://doi.org/10.1175/JAS-D-14-0164.1, 2014.

Kawatani, Y., Hamilton, K., Sato, K., Dunkerton, T. J., Watanabe, S., and Kikuchi, K.: ENSO Modulation of the QBO: Results from MIROC Models with and without Nonorographic Gravity Wave Parameterization, J. Atmos. Sci., 76, 3893–3917, https://doi.org/10.1175/JAS-D-19-0163.1, 2019.

Labitzke, K.: On the interannual variability of the middle stratosphere during the northern winters, J. Meteorol. Soc. Jpn., 80, 963–971, http://doi.org/10.2151/jmsj1965.60.1_124, 1982.

Lait, L. R., Schoeberl, M. R., and Newman, P. A.: Quasi-biennial modulation of the Antarctic ozone depletion, J. Geophys. Res., 94, 11559–11571, http://dx.doi.org/10.1029/JD094iD09p11559, 1989.

Li, F., Austin, J., and Wilson, R. J.: The strength of the Brewer–Dobson circulation in a changing climate: Coupled chemistry–climate model simulations, J. Climate, 21, 40–57, https://doi.org/10.1175/2007JCLI1663.1, 2008.

Liess, S. and Geller, M. A.: On the relationship between QBO and distribution of tropical deep convection, J. Geophys. Res., 117, D03108, http://dx.doi.org/10.1029/2011JD016317, 2012.

Lindzen, R. S.: Equatorial planetary waves in shear: Part I, J. Atmos. Sci. 28, 609-622, https://doi.org/10.1175/1520-0469(1971)028%3C0609:EPWISP%3E2.0.CO;2, 1971.

Lindzen, R. S. and Holton, J. R.: A theory of the quasi-biennial oscillation, J. Atmos. Sci., 25, 1095–1107, https://doi.org/10.1175/1520-0469(1968)025%3C1095:ATOTQB%3E2.0.CO;2, 1968.

Marshall, A. G. and Scaife, A. A.: Impact of the QBO on surface winter climate, J. Geophys. Res., 114, D18110, http://dx.doi.org/10.1029/2009JD011737, 2009.

Match, A., and Fueglistaler, S.: The buffer zone of the quasi-biennial oscillation, J. Atmos. Sci., 76, 3553–3567, https://doi.org/10.1175/JAS-D-19-0151.1, 2019

Match, A., and Fueglistaler, S.: Mean-flow damping forms the buffer zone of the quasi-biennial oscillation: 1D theory. J. Atmos. Sci., 77, 1955–1967, https://doi.org/10.1175/JAS-D-19-0293.1, 2020.

Matsuno, T.: Numerical integrations of primitive equations by use of a simulated backward difference method, J. Meteor. Soc. Japan, 44, 76–84, https://doi.org/10.2151/jmsj1965.44.1_76, 1966

Plass, G. N.: The influence of the 15μ carbon-dioxide band on the atmospheric infra-red cooling rate, Quart. J. Roy. Meteor. Soc., 82, 310–324, https://doi.org/10.1002/qj.49708235307, 1956.

Plumb, R. A.: The interaction of two internal waves with the mean flow: Implications for the theory of the quasi-biennial oscillation, J. Atmos. Sci., 34, 1847–1858, https://doi.org/10.1175/1520-0469(1977)034<1847:TIOTIW>2.0.CO;2, 1977.

Reed, R. J., Campbell, W. J., Rasmussen, L. A., and Rogers, D. G.: Evidence of a downward-propagating, annual wind reversal in the equatorial stratosphere, J. Geophys. Res., 66, 813–818, http://dx.doi.org/10.1029/JZ066i003p00813, 1961.

Richter, J. H., Anstey, J. A., Butchart, N., Kawatani, Y., Meehl, G. A., Osprey, S., & Simpson, I. R., 2020b: Progress in simulating the quasi-biennial oscillation in CMIP models. Journal Geophysical Research: Atmospheres, 125, e2019JD032362, https://doi.org/10.1029/2019JD032362, 2020a.

Richter, J. H., Butchart, N., Kawatani, Y., Bushell, A. C., Holt, L., Serva, F., Anstey, J., Simpson, I. R., Osprey, S., Hamilton, K., Braesicke, P., Cagnazzo, C., Chen, C.-C., Garcia, R. R., Gray, L. J., Kerzenmacher, T., Lott, F., McLandress, C., Naoe, H., Scinocca, J., Stockdale, T. N, Versick, S., Watanabe, S., Yoshida, K., Yukimoto, S.: Response of the Quasi-Biennial Oscillation to a warming climate in global climate models, Q. J. R. Meteorol. Soc., 1–29. https://doi.org/10.1002/qj.3749, 2020b.

Rind, D., Jonas, J., Balachandran, N., Schmidt, G., and Lean, J.: The QBO in two GISS global climate models: 1. Generation of the QBO, J. Geophys. Res. Atmos., 119, 8798–8824, https://doi.org/10.1002/2014JD021678, 2014.

Rind, D., Orbe, C., Jonas, J., Nazarenko, L., Zhou, T., Kelley, M., Lacis, A., Shindell, D., Faluvegi, Russell, G., Bauer, M., Schmidt, G., Romanou, A., and Tausnev, N.: GISS Model E2.2: A climate model optimized for the middle atmosphere — Model structure, climatology, variability and climate sensitivity, J. Geophys. Res. Atmos., 125, e2019JD032204, https://doi.org/10.1029/2019JD032204, 2020.

Saravanan, R.: A multiwave model of the quasi-biennial oscillation, J. Atmos. Sci., 47, 2465–2474, https://doi.org/10.1175/1520-0469(1990)047%3C2465:AMMOTQ%3E2.0.CO;2, 1990.

Scaife, A. A., Butchart, N., Warner, C. D., Stainforth, D., Norton, W., and Austin, J.: Realistic quasi-biennial oscillations in a simulation of the global climate, Geophys. Res. Lett., 27, 3481–3484, https://doi.org/10.1029/2000GL011625, 2000.

Schirber, S., Manzini, E., Krismer, T. and Giorgetta, M.: The Quasi-Biennial Oscillation in a warmer climate: sensitivity to different gravity wave parameterizations, Climate Dynamics, 45, 825–836, https://doi.org/10.1007/s00382-014-2314-2, 2015.

578 Trepte, C. R. and Hitchman, M. H.: Tropical stratospheric circulation deduced from satellite aerosol data,
579 Nature, 355, 626–628, https://doi.org/10.1038/355626a0, 1992.
580 Watanabe, S. and Kawatani, Y.: Sensitivity of the QBO to mean tropical upwelling under a changing
581 climate simulated with an Earth System Model, Journal of the Meteorological Society of Japan,
582 Series II, 90A, 351–360, https://doi.org/10.2151/jmsj.2012-A20, 2012.
583 Yoo, C. and Son, S.-W.: Modulation of the boreal wintertime Madden-Julian oscillation by the
584 stratospheric quasi-biennial oscillation, Geophys. Res. Lett., 43, 1392–1398,
585 https://doi.org/10.1002%2F2016GL067762, 2016.
586 Zawodny, J. M. and McCormick, M. P.: Stratospheric Aerosol and Gas Experiment II measurements of
587 the quasi-biennial oscilla- tions in ozone and nitrogen dioxide, J. Geophys. Res., 96, 9371– 9377,
588 http://dx.doi.org/10.1029/91JD00517, 1991.

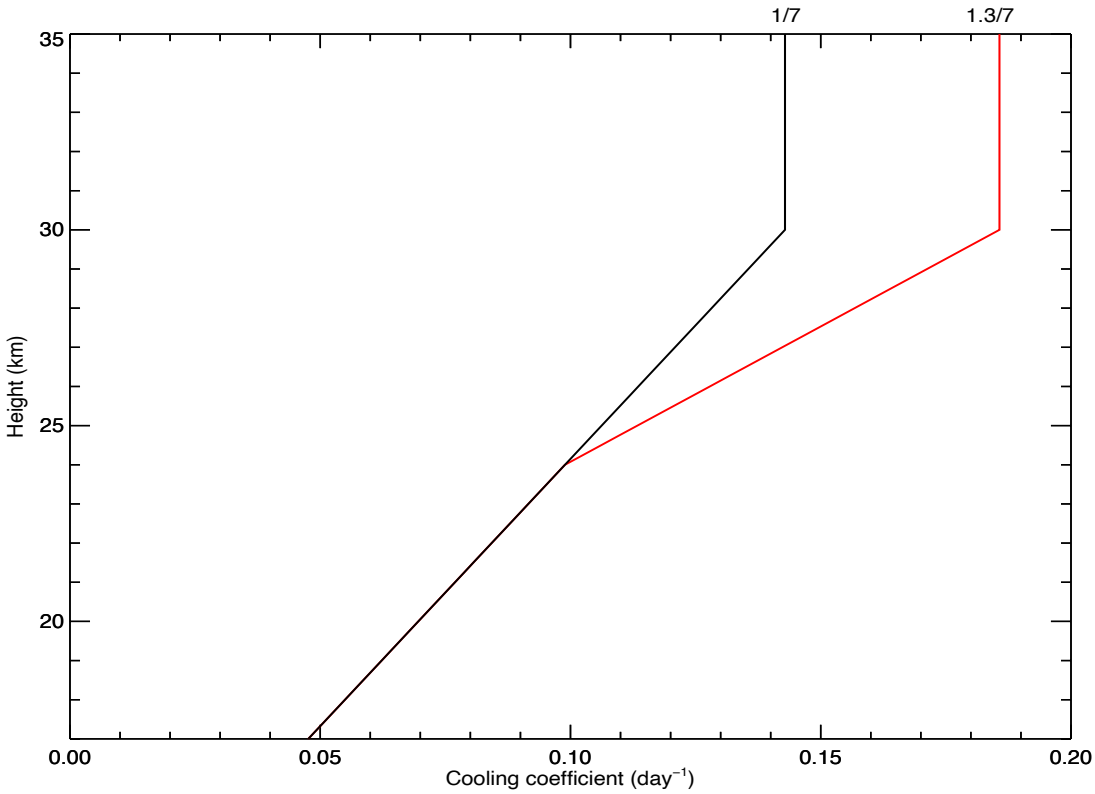

FIG. 1: Newtonian cooling profiles: The smaller values (black line) are used for the control runs while the larger values (red line) are used for the experimental runs.

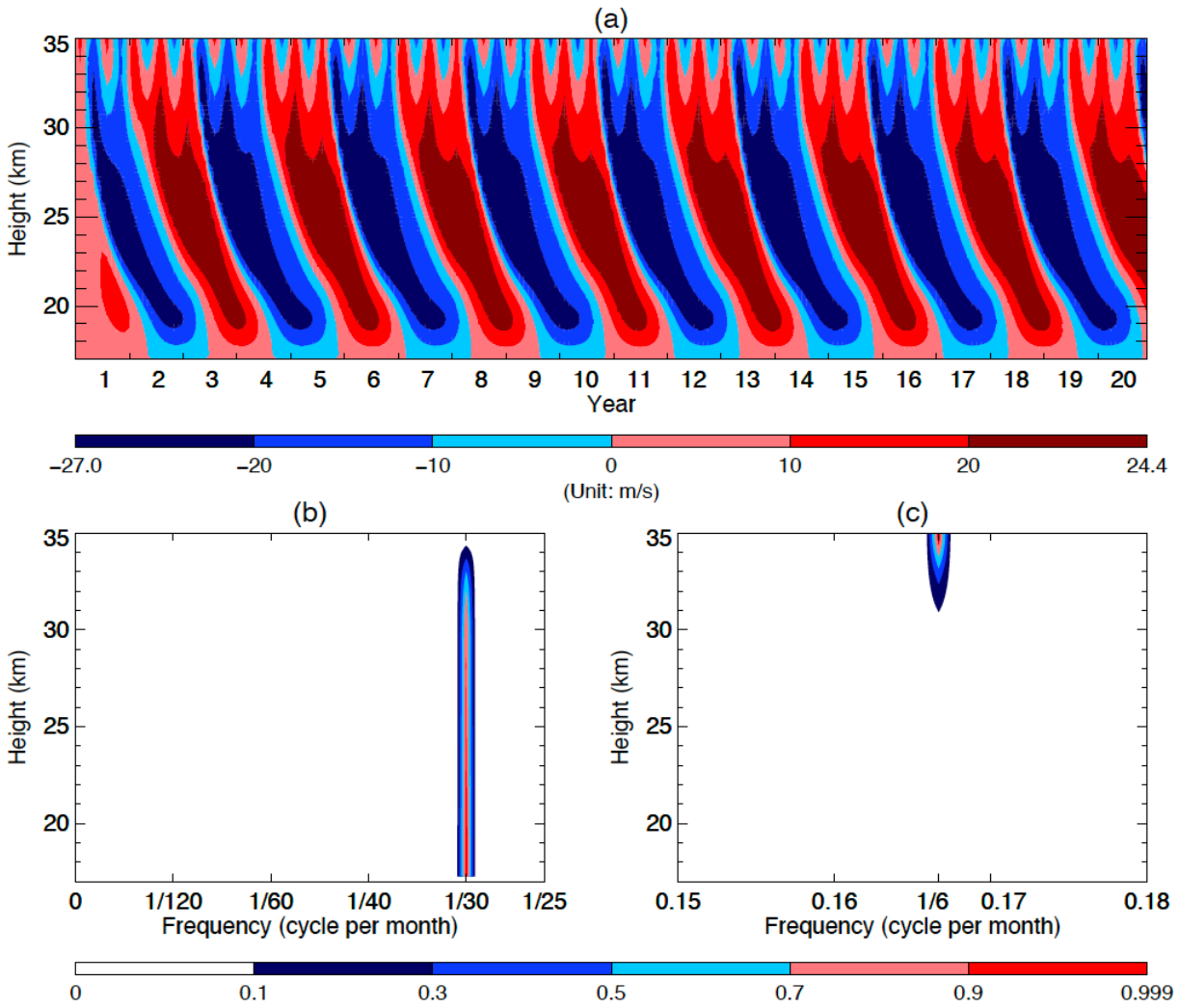

FIG. 2: (a) Time–height section of the monthly averaged mean zonal wind over the first 20 years from the HL's original model. (b) and (c) Frequency–height section of the power spectral densities (PSD) of the standardized monthly averaged mean zonal wind of the 100 years. Note that in order to better visualize the PSD in (b) and (c), we trimmed off the blank segments for the frequencies ranging from $\frac{1}{25}$ to 0.15 cycle per month and those ranging from 0.18 to 0.5 cycle per month.

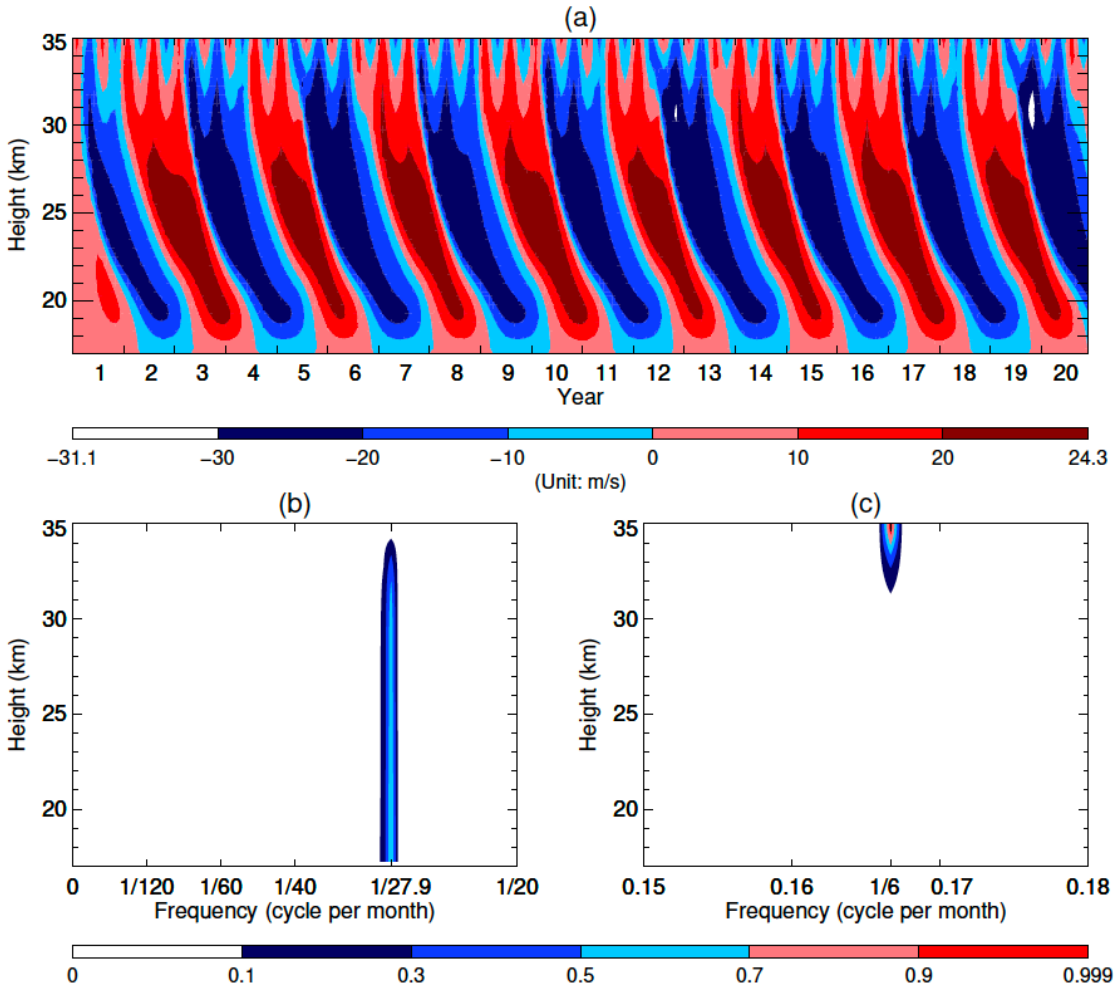

FIG. 3: (a) Same as FIG. 2a, but with the enhanced $\alpha(z)$ depicted as the red line in FIG. 1. (b) and (c) Frequency–height section of the power spectral densities (PSD) of the standardized monthly averaged mean zonal wind of the 100 years. Note that in order to better visualize the PSD in (b) and (c), we trimmed off the blank segments for the frequencies ranging from $\frac{1}{20}$ to 0.15 cycle per month and those ranging from 0.18 to 0.5 cycle per month.

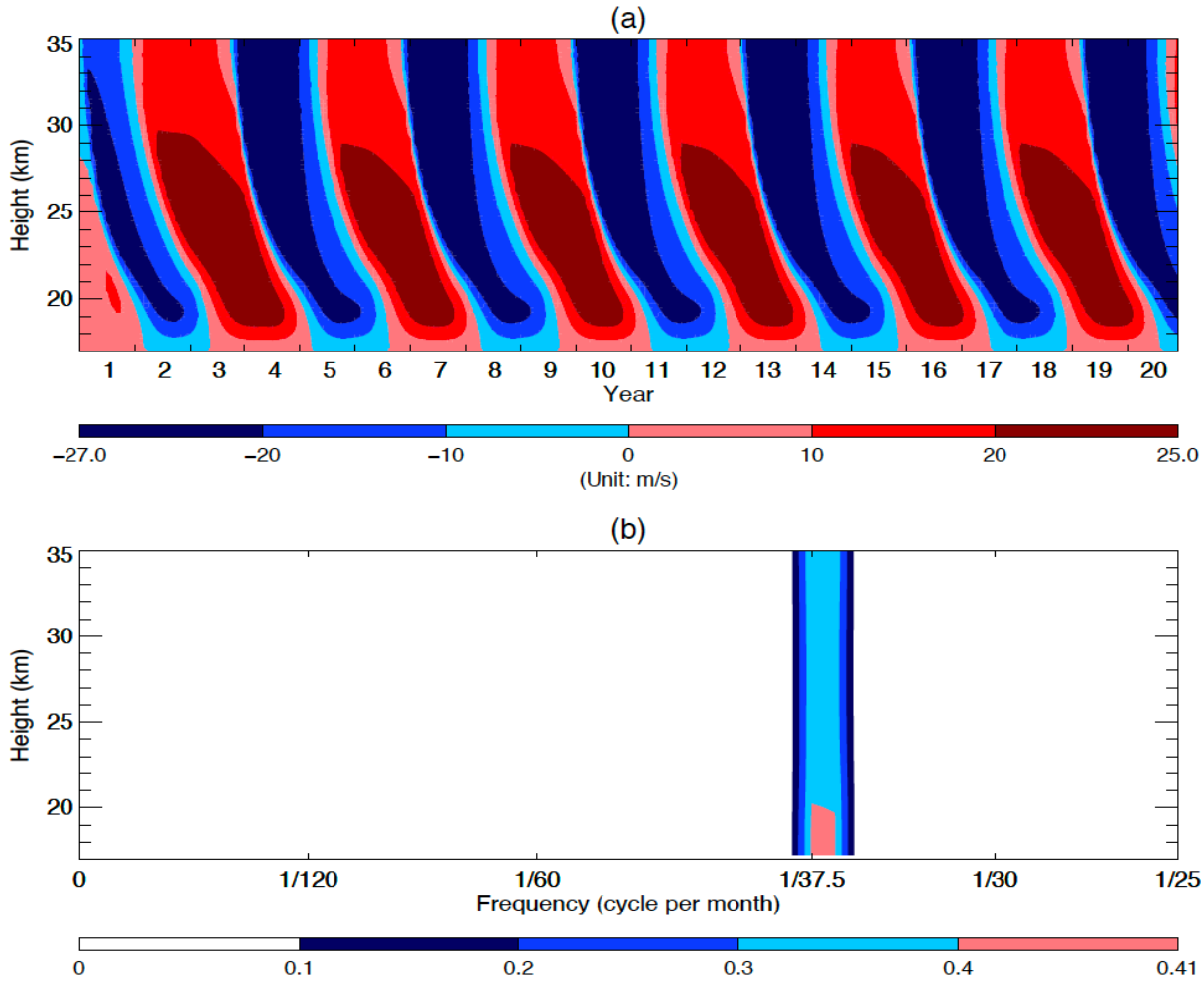

FIG. 4: (a) Time–height section of the monthly averaged mean zonal wind over the first 20 years from the HL's model without the semiannual forcing. (b) Frequency–height section of the power spectral densities (PSD) of the standardized monthly averaged mean zonal wind of the 100 years. Note that in order to visualize the PSD, we trimmed off the blank segment for the frequencies ranging from $\frac{1}{25}$ to 0.5 cycle per month.

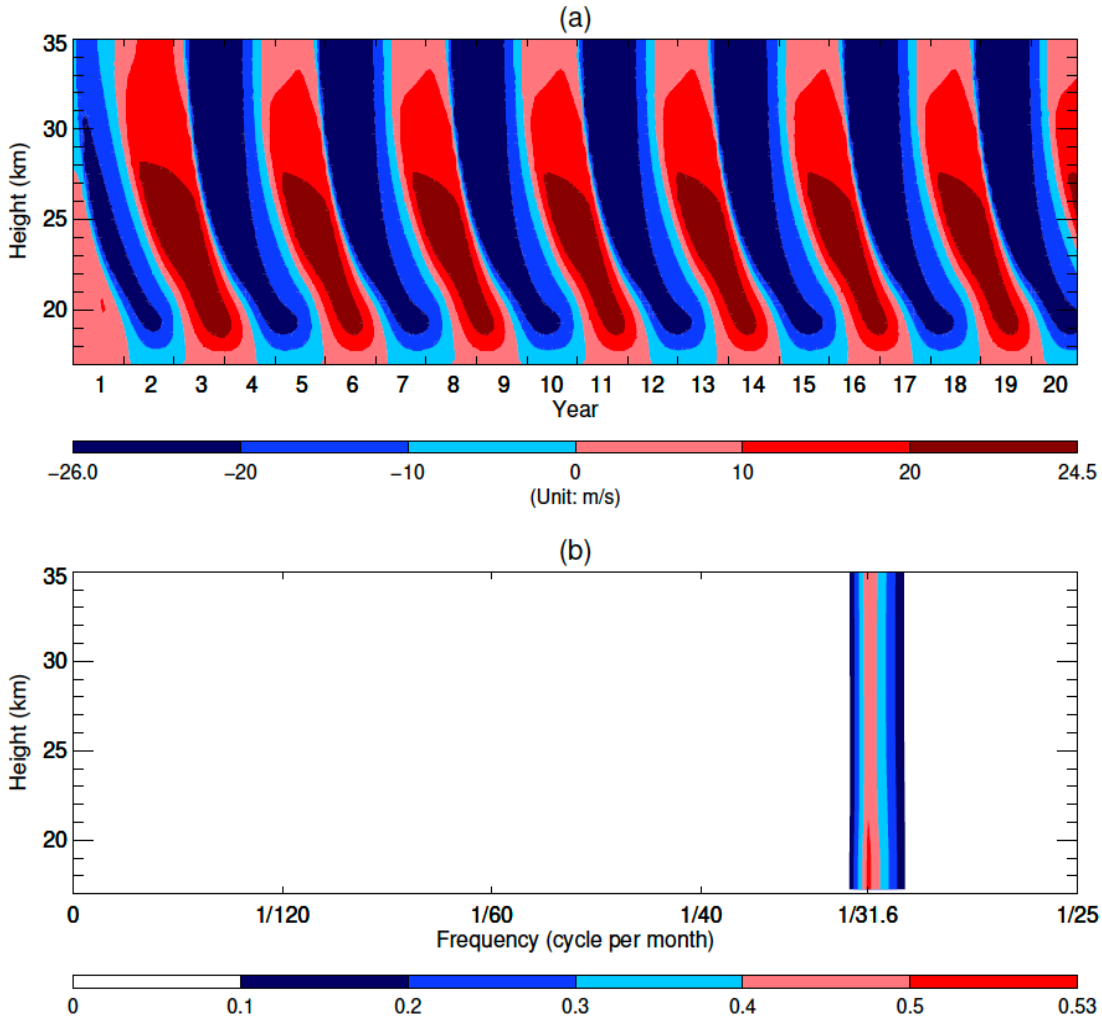

FIG. 5: (a) Same as FIG. 4a, but with the enhanced $\alpha(z)$ depicted as the red line in FIG. 1. (b) Same as FIG. 4b, but for the doubled CO_2 Run.

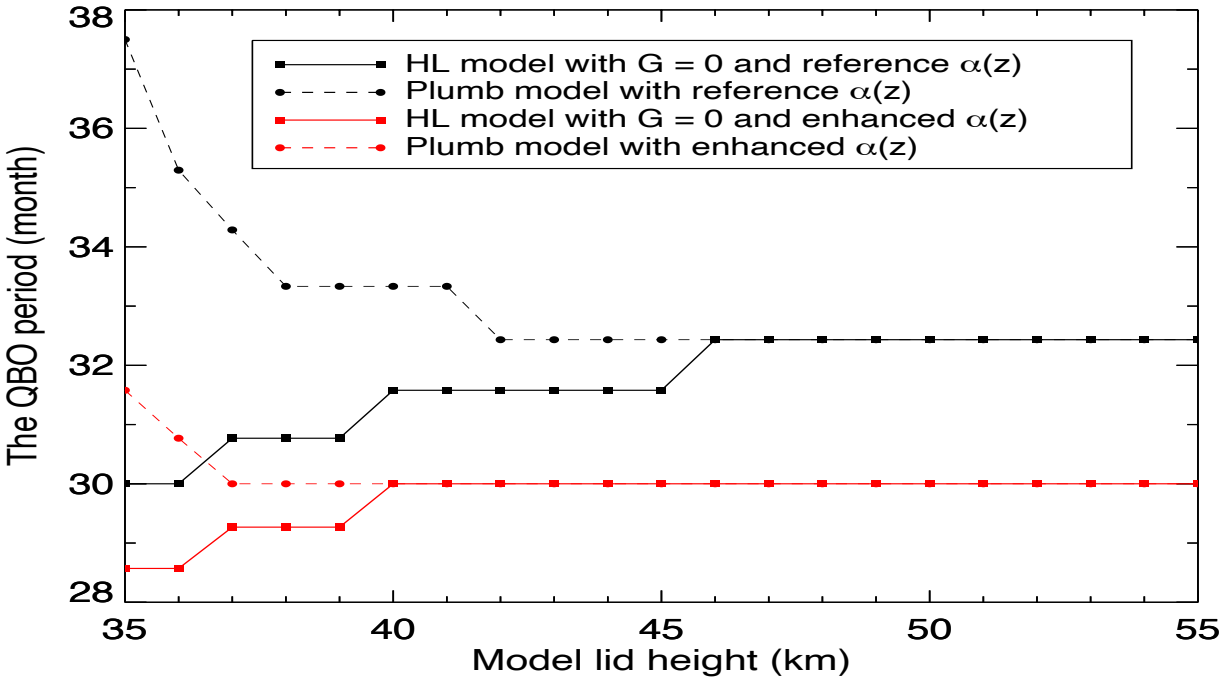

FIG. 6: The relationship between the simulated QBO period with the height of the model lid. Black and red lines depict the results from using the reference radiative damping and the enhanced radiative damping respectively while solid and dashed lines delineate the results from the HL model with $G = 0$ and the Plumb model respectively.